REPORT DOCUMENTATION PAGE

1. REPORT DATE (DD-MM-YYYY)	2. REPORT TYPE	3. DATES COVERED (From - To)
21072005	Journal Article	

4. TITLE AND SUBTITLE

Flow response of a segregating mixture by interacting lattice gas simulation

5a. CONTRACT NUMBER

5b. GRANT NUMBER

5c. PROGRAM ELEMENT NUMBER

6. AUTHOR(S)

R.B. Pandey, J.F. Gettrust

5d. PROJECT NUMBER

5e. TASK NUMBER

5f. WORK UNIT NUMBER

7. PERFORMING ORGANIZATION NAME(S) AND ADDRESS(ES)

Naval Research Laboratory
Seafloor Sciences Branch
Stennis Space Center, MS 39529

8. PERFORMING ORGANIZATION REPORT NUMBER

NRL/JA/7430-05-1

9. SPONSORING/MONITORING AGENCY NAME(S) AND ADDRESS(ES)

Office of Naval Research
800 North Quincy Street
Arlington, VA 22217-5660

10. SPONSOR/MONITOR'S ACRONYM(S)

ONR

11. SPONSOR/MONITOR'S REPORT NUMBER(S)

12. DISTRIBUTION/AVAILABILITY STATEMENT

Approved for public release; distribution is unlimited

13. SUPPLEMENTARY NOTES

Physica A 358 (2005) 437-446

14. ABSTRACT

Steady-state flow and structural profiles of immiscible components A and B (molecular weights M_A and M_B, $M_A < M_B$) in a non-conservative open system are studied by an interacting lattice gas Monte Carlo simulation. Concentration gradient and hydrostatic bias H drive the constituents (A, B) which are continuously released from the bottom with equal probability against gravity. At low bias, the segregation of A and B leading to a partial layering is enhanced toward the bottom. The longitudinal density profile with a high density in the bottom region and low toward the top shows linear, exponential, and power-law decays in different regions of depth or altitude which varies systematically with the pressure bias. The transverse density profiles show segregation with different domain sizes and layering depending on the bias. Response of their steady-state flux density j to the hydrostatic bias

15. SUBJECT TERMS

Lattice gas; Mixture; Segregation; Non-equilibrium steady state; Linear response

16. SECURITY CLASSIFICATION OF:			17. LIMITATION OF ABSTRACT	18. NUMBER OF PAGES	19a. NAME OF RESPONSIBLE PERSON
a. REPORT	b. ABSTRACT	c. THIS PAGE	SAR	10	Ras Pandey
Unclassified	Unclassified	Unclassified			19b. TELEPHONE NUMBER (Include area code) 228-688-5480

ELSEVIER

Flow response of a segregating mixture by interacting lattice gas simulation

R.B. Pandey[a,b,*], J.F. Gettrust[a]

[a]*Naval Research Laboratory, Stennis Space Center, MS 39529, USA*
[b]*Department of Physics and Astronomy, University of Southern Mississippi, Hattiesburg, MS 39406-5046, USA*

Abstract

Steady-state flow and structural profiles of immiscible components A and B (molecular weights M_A and M_B, $M_A < M_B$) in a non-conservative open system are studied by an interacting lattice gas Monte Carlo simulation. Concentration gradient and hydrostatic bias H drive the constituents (A, B) which are continuously released from the bottom with equal probability against gravity. At low bias, the segregation of A and B leading to a partial layering is enhanced toward the bottom. The longitudinal density profile with a high density in the bottom region and low toward the top shows linear, exponential, and power-law decays in different regions of depth or altitude which varies systematically with the pressure bias. The transverse density profiles show segregation with different domain sizes and layering depending on the bias. Response of their steady-state flux density j to the hydrostatic bias H is found to be linear at higher bias. The difference in response of the flux density of the two components becomes more pronounced at low bias and higher miscibility gap.
Published by Elsevier B.V.

A continuous release of constituents (particles (A, B)) from a source into the bottom of an effective open medium leads to its steady-state flow. How much the net

*Corresponding author. Tel.: +601 266 4485; fax: +601 266 5149.
E-mail address: ras.pandey@usm.edu (R.B. Pandey).

amount of A and B flows and how their density profiles appear, depends not only on the rate of release but also on the type of constituents (i.e., immiscibility), their interaction with the effective medium (i.e., miscibility), sedimentation and precipitation (due to molecular weight), pressure bias (driving field), etc. In order to gain a systematic understanding of evolving morphologies and their flow, one has to narrow down the parameter space. For example, we can fix the rate of release of constituents from the source and their molecular weights (i.e., $M_A/M_B = \frac{1}{3}$) and vary the pressure bias (H). One may study the effect of miscibility by changing the interaction strength among the constituents (AA, AB, BB) and with the effective medium (AS, BS), i.e., with the empty lattice sites (S). Identifying the qualitative trend from the unscaled quantitative data generated by computer simulations is one of our objectives in this article.

The global (and local) structure evolving from individual interacting components and their flow share some general characteristics, at least in part with many systems such as flow of immiscible fluid mixture (oil and water) into a miscible solvent, flow of methane gas and hydrocarbon, and dissociation of hydrates in aqueous environments [1]. Our main interest, however, is focused on understanding the flow of a mixture of methane gas along with other components (i.e., immiscible hydrocarbon) below the ocean floor to sub-bottom area in aqueous and dynamic sedimentary environment [2–5]. In the long term, we are interested in a comprehensive understanding of the effects of driving fields such as concentration gradients, hydrostatic pressure, thermal gradient, etc. [6,7] which are crucial in understanding the hydrate formation, mound evolution, dissociation leading to such instabilities as mud volcanoes [8–10] below the ocean floor. We recently reported [11] the onset of segregation with partial layered patterns in a steady-state flow. Changes in concentration/density profiles with the hydrostatic pressure bias were also examined very recently [12] for immiscible mixtures (A, B) with a range of molecular weight ratios ($M_B/M_A = 1 - 10$). Attempts were made to quantify the variations of the overall steady-state density of these constituents and their scaling with the bias (H) and the molecular weight. In this article, we study the response of flow to bias with steady-state structures involving segregation where both constituents are released from the source regardless of their overall concentration in the system.

The mixture consists of interacting particles which are driven by hydrostatic bias and concentration gradient against gravitational forces while they aggregate and segregate. Such non-equilibrium steady-state systems provide a wide range of structural patterns. Effects of external driving field/force on ordering and non-equilibrium phase transition in conservative particles systems (with constant number of constituents) are studied extensively with a long list of literature [13,14]. Investigations of structures and patterns in granular driven systems [15,16] have attracted a considerable interests in recent years [17–23]. Understanding the global patterns from the mobility of individual constituents are difficult to monitor experimentally [24]. However, it is relatively easier to investigate flow and patterns [25,26] in such a complex particulate mixture by computer simulation methods such as lattice gas [27,28], molecular dynamics [29,30], and Monte Carlo [31] methods. Most of the particulate driven system [13–23] deal with conservative systems with a

constant number of constituents. Unlike Boltzmann lattice gas [32], it is easier to incorporate interactions between constituent particles and effective medium (empty lattice sites, see below) in interacting lattice gas. We use an interacting lattice gas Monte Carlo simulation here to study the flow response in a steady-state mixture with non-conservative constituents as follows.

As before [11,26], we consider a cubic lattice of size L^3 with $L = 30-400$ with a source of particles A and B connected to the bottom of the lattice ($z = 1$). About half of the lattice sites are initially occupied by A or B randomly with equal probability. The empty sites represent the effective solvent (S) medium. The steady-state global properties do not depend on the initial configuration (see below). The interaction energy U between these components is described by

$$U = \sum_i \sum_k J(i,k), \tag{1}$$

where index i runs over all particles and k over all nearest neighbor sites of i with,

$$J(A,A) = J(B,B) = -J(A,B) = -J(B,A) = -\varepsilon_1, \tag{2}$$

$$J(A,S) = J(B,S) = -\varepsilon_2. \tag{3}$$

The positive miscibility gaps ($\varepsilon_1 = 1, 2$) considered here, enhance the phase separation between A and B in contrast to their mixing with the solvent $\varepsilon_2 = 1$.

Downward fall, i.e., sedimentation is controlled by the molecular weights of constituents ($M_A = 0.1, M_B = 0.3$) via change in the gravitational potential energy as they move down ($-z$) or up ($+z$). In addition to high concentration gradient at the bottom due to source, a hydrostatic pressure bias (H) is considered to drive the constituents upward against gravity. The Metropolis algorithm is used to move randomly selected particles to their nearest neighbor sites selected randomly with following probabilities along the transverse ($\pm x, \pm y$) and vertical ($\pm z$) directions:

$$P_x = P_{-x} = P_y = P_{-y} = \frac{1}{6}; \quad P_z = \frac{1+H}{6}, \quad P_{-z} = \frac{1-H}{6}; \quad 0 \leqslant H \leqslant 1. \tag{4}$$

Periodic boundary conditions are used along the transverse direction; both top ($z = L$) and bottom ($z = 1$) of the sample are open for particles to escape. A particle (A or B with equal probability) is released into a bottom lattice site as soon as it is vacated by the particle when it moves up or diffuses laterally. As usual, the attempt to move each particle once defines the unit Monte Carlo step (MCS) time.

As the simulation proceeds, particles (A, B) move in and out of the sample. The number of particles and their concentration profiles (planar densities along x, y, z) change but eventually reach a steady-state—a non-equilibrium steady-state system. Simulations are performed with many independent samples each for a sufficiently long time steps to reach steady state. We have observed [11] evolution of interesting structural patterns, i.e., onset of phase separation, oscillation in lateral density profiles, layering, etc. These structural patterns share some characteristics of granular systems studied in recent years [33–35]. In the following, we focus mainly on the global transport and flow response in segregating steady-state patterns.

Simulations are performed on various lattice sizes 30^3–400^3 with most production runs on 30^3, 50^3, and 100^3 lattices using as many as 128 independent runs for the range of pressure bias $H = 0.0-1.0$. Finite size effects on the qualitative behavior of the physical quantities are negligible particularly with 50^3 and 100^3 samples except for few runs at low bias values. The miscibility gaps are restricted to $\varepsilon_1 = 1.0$, 2.0, and $\varepsilon_2 = 1.0$ with the molecular weights $M_A = 0.1$, $M_B = 0.3$, and temperature $T = 1.0$ in arbitrary units of interaction energy and Boltzmann constant.

Fig. 1 shows the steady-state density profiles in the whole range of pressure bias. The longitudinal profiles with altitude clearly show a decay of the density with the height (z): sharp decline at low height is followed by a slow but linear decay at the intermediate height before a sharp decline again toward the top. The density profiles depend on the magnitude of the bias. The density of heavier component (B) is generally higher particularly at lower bias and low altitudes. At extreme values of bias ($H \rightarrow 1$), the density profiles of both components approach the same shape. Attempts are made to explore the exponential (log-normal scale) and log–log (Fig. 2) fits which suggest that the steady-state variation of the density of each component depend on the range of altitude, magnitude of the bias, and the molecular weight of the components. For example, at the high value of the bias ($H = 1.0$) where the
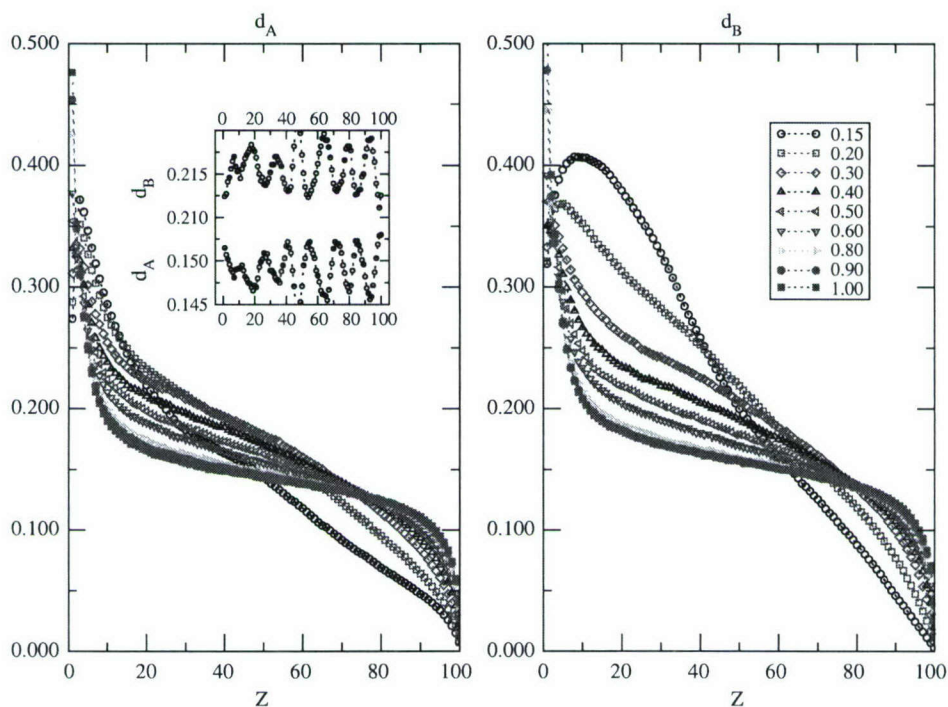

Fig. 1. Density (d_A, d_B) profiles of A and B components at a range of bias $H = 0.15-1.00$. The inset shows a transverse (Y) density profile at $H = 0.15$. Sample size 100^3 is used with 32–128 runs.
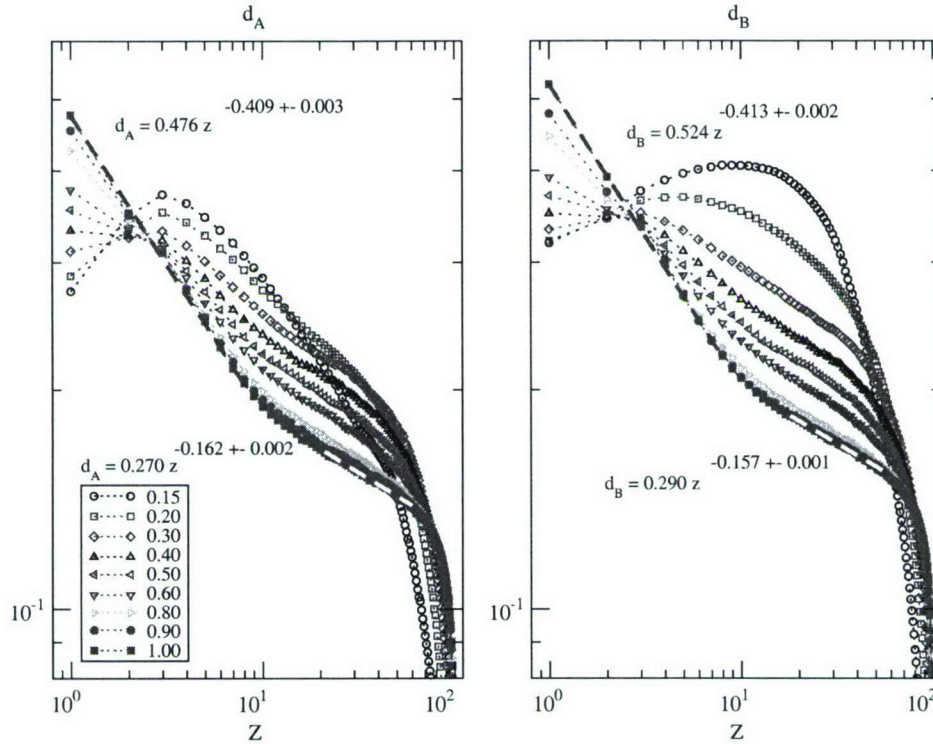
Fig. 2. Density (d_A, d_B) profiles of A and B components at a range of bias $H = 0.15-1.00$ on log–log scale to search for a power-law dependence. Sample size 100^3 is used with 32–128 runs (Fig. 1 on a different scale).

density profiles of A and B are similar (see Fig. 2), a sharp power-law decay of density with the altitude (at $Z \simeq 1-8$) is followed by a slower power-law decay ($Z \simeq 15-80$) before dropping precipitously toward the top ($Z \simeq 90-100$). The power-law decay (Fig. 2) at $H = 1.0$, $d_{A/B} \propto z^{-0.4}$ at lower altitude is followed by $d_{A/B} \propto z^{-0.2}$ at higher altitude. Note that the power-law exponent depends on the pressure bias and range of the altitude. Particularly at low bias values, a range of power-law decays including non-monotonic variation of densities with z is seen where concentration gradient seems to dominate the driving forces.

Toward the bottom end where both components have higher densities, it is easier to identify the structural changes due to their interaction (i.e., miscibility). The density profile is important as its gradient provides one of the driving bias for the mass transfer from bottom to top. The transverse density profile provides insight into the lateral distribution of their constituents which affect their transverse mobility (see below). In fact, the phase separation between A and B is most visible at low values of bias ($H = 0.0-0.30$); a transverse profile is shown in the inset of Fig. 1 at $H = 0.15$. The complementary and somewhat oscillatory variation in the

density of B (higher) and A (lower) exhibits segregation with onset of their layering toward the bottom planes (also seen in visualization). The segregated layers smear out toward the upper half where their density become much smaller.

Although each particle (A, B) attempts to move, particles at the top (low-density phase) are much more mobile than those toward the bottom (high-density phase). The motion of each particle may not be as insightful as the overall motion of their center of mass for the net flow. Fig. 3 shows variation of the longitudinal component of the mean square displacement on a log–log scale for the whole range of bias; variation of the representative transverse (y) component is presented in the inset. The power-law behavior is observed even at the lowest value the bias ($H = 0.15$) in the asymptotic time limit. Despite similarity in the power-law dependence, there are considerable differences in their magnitude (R_z^2); i.e., it is higher for the lighter (A) component particularly at low bias. However, the variation with bias is more pronounced for the heavier component (B). Note the contrast in the order of magnitude of longitudinal (R_z^2) and transverse (R_y^2) components: the extremely low values of R_y^2 show very low overall mobility of the center of mass along the transverse direction while the comparatively high magnitude of R_z^2 show a large transport along vertical direction.
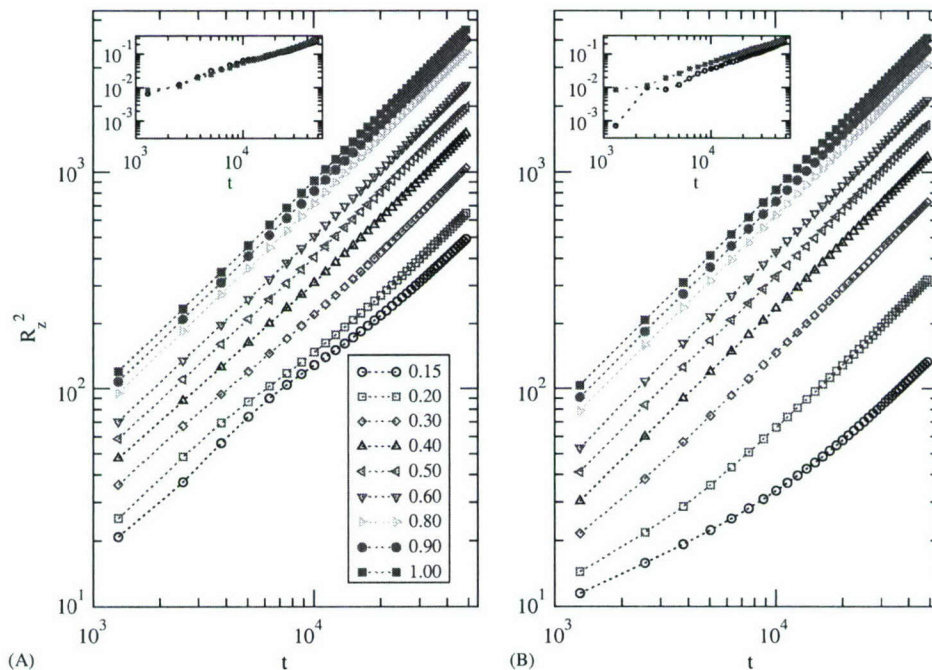

Fig. 3. Mean square displacement (longitudinal component R_z^2) versus time steps for components A and B; variation of a transverse (R_y^2) component is presented in the inset at extreme values of $H = 0.15, 1.00$. Statistics is the same as Fig. 1.

The constant in-flux of constituents from the source at the bottom in presence of an upward pressure bias provides their net flow (i.e., mass transfer) despite gravitational forces. In steady state, the output from the top must be equal to net input flow at the bottom as the conservation of mass leads to continuity equation. The rate (j) of mass transfer per unit cross-sectional area (A_c) defines the flux density,

$$j = \frac{1}{A_c} \frac{dQ}{dt} \, ,$$

(5)

where $A_c = L_x \times L_y$ and Q is the net mass transfer at time step t. In the steady state the flux density from the top and bottom should be equal. Variation of the flux density with the time steps for both components is presented in Fig. 4 which is consistent with

$$j_{top} = j_{bottom}$$

(6)

in the long time limit. The approach to steady state depends on the bias, the larger is the bias, the faster is the approach to steady state.

One would expect the flux density to increase on raising the driving bias. In addition to the pressure bias (H), the concentration gradient also drives the
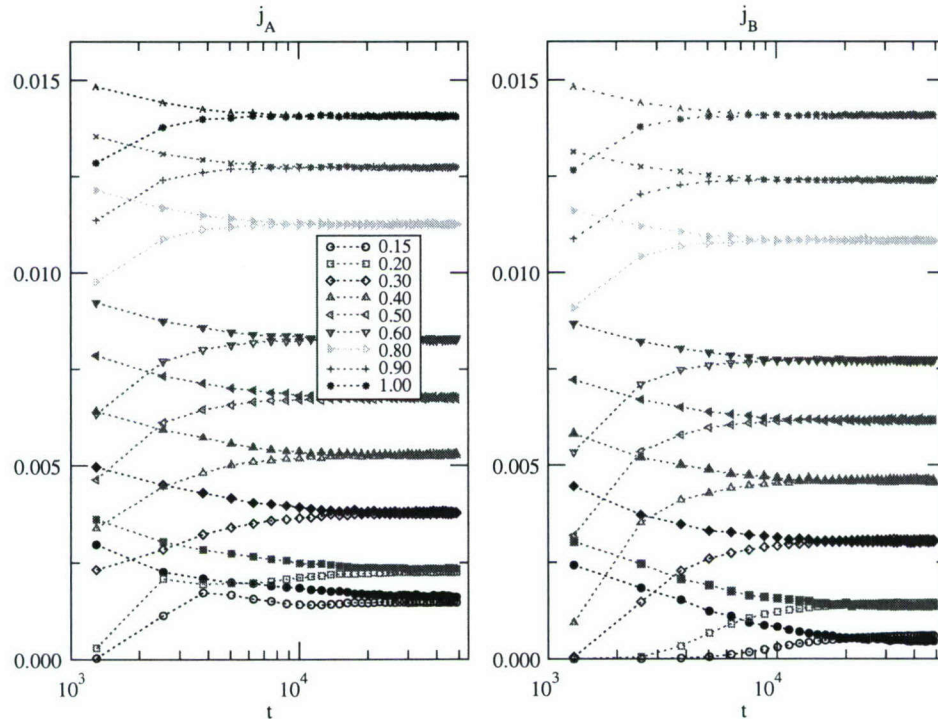

Fig. 4. Flux density versus time steps at various bias. Upper data points are the flux density from the bottom and lower points are for flux density from the top. Statistics is the same as Fig. 1.

constituents upward against gravitational force. Since, the downward gravitational bias (which depends on the molecular weight of constituents) is constant, and it is difficult to quantify the overall bias due to concentration gradient, the response of the flux density j to the driving field is examined by varying the pressure bias (H). Fig. 5 shows the variation of the flux density j with bias H, for different sample sizes and interaction parameter $\varepsilon_1 = 1, 2$ for the miscibility gap. In the high range of bias, the response of j to H is linear and is less sensitive to miscibility gap. In the low-bias regime, there is deviation on increasing the miscibility gap from $\varepsilon_1 = 1$ to 2. The response at low values of H differs from that in the high range of bias. Effects of gravitational forces and the concentration gradient are clearly more visible at low values of pressure bias. Further, the effect of molecular weight ($M_A < M_B$) on the
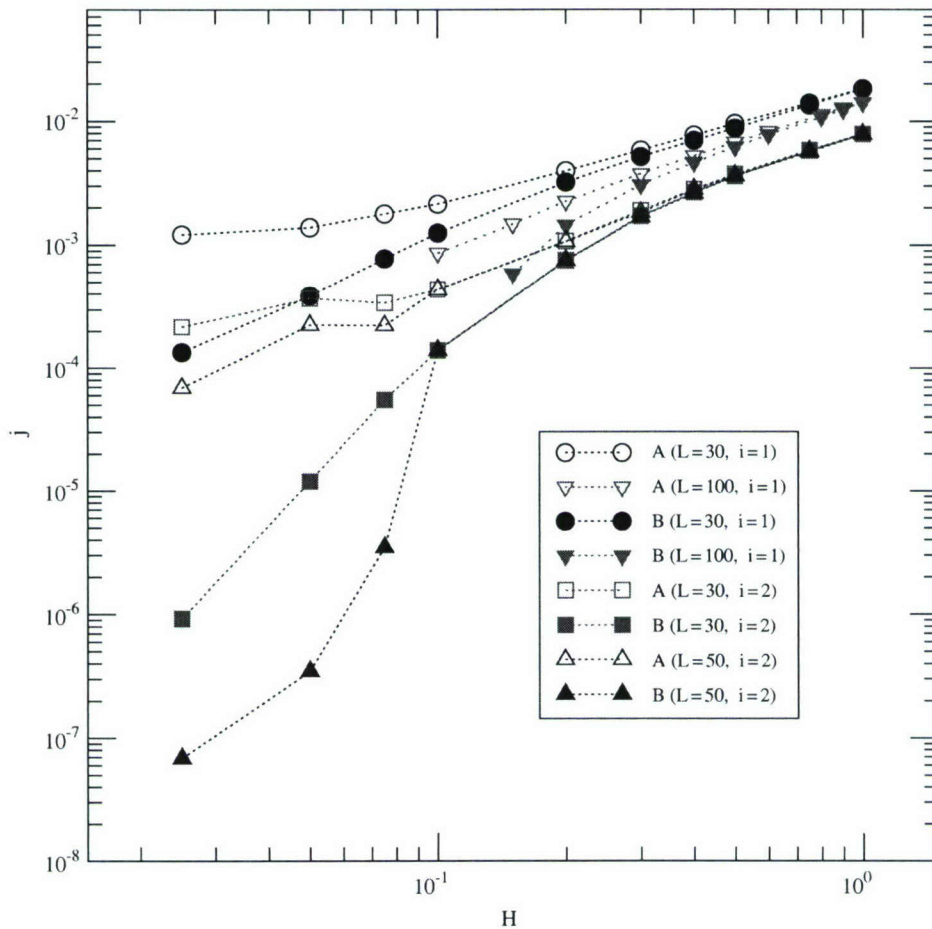

Fig. 5. Variation of the steady-state flux density with the pressure bias H with different sample sizes ($L = 30, 50, 100$) and miscibility gap $\varepsilon_1 = i = 1, 2$. The number of independent runs varies from 10 ($L = 30, 50$) to 128 ($L = 100$) sizes.

response is also significant particularly at low-pressure bias: A component responds faster than B as $j_A \geqslant j_B$. Within the statistical fluctuations, there is hardly any finite size effect on the qualitative nature of the response.

In summary, an interacting lattice gas computer simulation model is used to study the flow response of immiscible components (A, B) which are constantly released with equal probability from the source at the bottom and driven by an upward bias against gravitational force. The number of particles is not conserved as they escape from the top and leak from the bottom. These interacting constituents in an effective medium are continuously driven out of equilibrium by the bias but their concentration profile and flux density reach steady state. The longitudinal density profile with a high density in the bottom region and low toward the top shows linear, exponential, and power-law decays in different regions of depth or altitude which varies systematically with the pressure bias. The transverse density profiles show segregation with different domain sizes depending on the bias. The flux density (j_A, j_B) of both constituents respond linearly to pressure bias in the high-bias regime in which $j_A \sim j_B$ as $H \to 1$. The difference in flow response increases on reducing the bias. In the low-bias region, the response of flux density of the component (B) with the higher molecular weight is lower than that of the lighter constituents (A). The flux density response is also found to be lower with higher miscibility gap in the low-bias region where not only the response is different from that in the high-bias region, but also signals a deviation from a linear response.

References

[1] Proceeding of the Fourth International Conference on Gas Hydrate, Yokohama, 2002.
[2] M.D. Max, S.T. Clifford, Geophys. Res. Lett. 28 (9) (2001) 1787–1790.
[3] W. Xu, R.P. Lowell, E.T. Peltzer, J. Geophys. Res. B: Solid Earth 106 (11) (2001) 26413–26423.
[4] E.D. Sloan, Clathrate Hydrates of Natural Gases, second ed., Marcel Dekker, New York, 1997.
[5] W.T. Wood, J.F. Gettrust, in: C.K. Paul, W.P. Dillon (Eds.), Natural Gas Hydrates: Occurrence, Distribution, and Dynamics, AGU Monograph, vol. 124, 2001, p. 165.
[6] Chuang Ji, G. Ahmadi, W. Zhang, D.H. Smith, in: Proceeding of the Fourth International Conference on Gas Hydrate, Yokohama, 2002, p. 791.
[7] Hisashi O. Kono, B. Budhijanto, S. Narasimhan, D.H. Smith, in: Proceeding of the Fourth International Conference on Gas Hydrate, Yokohama, 2002, p. 543.
[8] R. Capozzi, V. Picotti, Terra Nova 14 (5) (2002) 363–370.
[9] G. Etiope, C. Baciu, A. Caracausi, R. Favara, F. Italiano, Geophys. Res. Lett. 29 (8) (2002) 56-1-56-4.
[10] T.K.P. Gregg, J.H. Fink, J. Volcanol. Geothermal Res. 96 (3–4) (2000) 145–159.
[11] R.B. Pandey, J.F. Gettrust, Ray Seyfarth, Luis A. Cueva-Parra, Int. J. Mod. Phys. C 14 (2003) 955.
[12] R.B. Pandey, J.F. Gettrust, Physica A 345 (2005) 555.
[13] B. Schmittmann, R.K.P. Zia, Statistical Mechanics of Driven Diffusive Systems, Academic Press, New York, 1995.

[14] J. Marro, R. Dickman, Nonequilibrium Phase Transitions in Lattice Models, Cambridge University Press, Cambridge, 1999.
[15] A. Mehta, (Ed.), Granular Matter: An Interdisciplinary Approach, Springer, New York, 1994.
[16] A. Coniglio (Ed.), Unifying Concepts in Granular Media and Glasses, Elsevier, Amsterdam, 2004.
[17] H.A. Makse, S. Havlin, P.R. King, H.E. Stanley, in: L. Schimansky-Geier, T. Poeschel (Eds.), Novel Pattern Formation in Granular Matter, Springer, Heidelberg, Berlin, 1997, p. 319.
[18] H.A. Makse, Physica A 330 (2003) 83.
[19] M. Latzel, S. Luding, H.J. Herrmann, Granular Matter 2 (2000) 123.
[20] D.C. Rapaport, Phys. Rev. E 65 (2002) 61306.
[21] P. Biswas, P. Sanchez, M.R. Swift, P.J. King, Phys. Rev. E 68 (2003) 050301.
[22] E. Villermaux, J. Duplat, Phys. Rev. Lett. 91 (2003) 184501.
[23] A.C. Lund, C.A. Schuh, Phys. Rev. Lett. 91 (2003) 23505.
[24] J. Geng, R.P. Behringer, Phys. Rev. Lett. 93 (2004) 238002.
[25] R. Consiglio, D.R. Baker, G. Paul, H.E. Stanley, Physica A 319 (2003) 49.
[26] R.B. Pandey, D. Stauffer, R. Seyfarth, Luis A. Cueva, J.F. Gettrust, Warren Wood, Physica A 310 (2002) 325.
[27] A. Xu, G. Gonnella, A. Lamura, Physica A 331 (2004) 10.
[28] L.O.E. Santos, P.C. Facin, P.C. Philippi, Phys. Rev. E 68 (2003) 056302.
[29] M.C. Mitchell, J.D. Autry, T.M. Nenoff, Molecular Phys. 99 (2001) 1831.
[30] G. Foffi, W. Gotze, F. Sciortino, P. Tartaglia, Th. Voigtmann, Phys. Rev. E 69 (2004) 011505.
[31] R. Finken, J.P. Hansen, A.A. Louis, J. Phys. A 37 (2004) 577.
[32] D.A. Wolf-Gladrow, Lattice Gas Cellular Automata and Lattice Boltzmann Models: An Introduction, Lecture Notes in Mathematics, Springer, Berlin, 2000.
[33] S. Aumaitre, T. Schnautz, C.A. Kruelle, I. Rehberg, Phys. Rev. Lett. 90 (2003) 144302.
[34] B. Meerson, T. Poschel, Y. Bromberg, Phys. Rev. Lett. 91 (2003) 024301.
[35] J.-C. Tsai, G.A. Voth, J.P. Gollub, Phys. Rev. Lett. 91 (2003) 064301.